

Baryon acoustic oscillations from Integrated Neutral Gas Observations: Broadband corrugated horn construction and testing

C. A. Wuensche^{1*} · L. Reitano¹ ·
M. W. Peel^{2,3,4} · I. W. A. Browne⁵ ·
B. Maffei⁶ · E. Abdalla² · C. Radcliffe⁷ ·
F. Abdalla⁸ · L. Barosi⁹ · V. Liccardo¹ ·
E. Mericia¹ · G. Pisano¹⁰ · C. Strauss¹ ·
F. Vieira¹ · T. Villela^{1,11} · B. Wang¹²

Received: date / Accepted: date

Abstract The Baryon acoustic oscillations from Integrated Neutral Gas Observations (BINGO) telescope is a 40-m class radio telescope under construction that has been designed to measure the large-angular-scale intensity of HI emission at 980–1260 MHz and hence to constrain dark energy parameters. A large focal plane array comprising of 1.7-metre diameter, 4.3-metre length corrugated feed horns is required in order to optimally illuminate the telescope. Additionally, very clean beams with low sidelobes across a broad frequency range are required, in order to facilitate the separation of the faint HI emission from bright Galactic foreground emission. Using novel construction methods,

C. A. Wuensche (orcid.org/0000-0003-1373-4719)
E-mail: ca.wuensche@inpe.br

¹Divisão de Astrofísica, Instituto Nacional de Pesquisas Espaciais (INPE), São José dos Campos, SP, Brazil

²Instituto de Física, Universidade de São Paulo, São Paulo - SP, Brazil

³Instituto de Astrofísica de Canarias, E-38205 La Laguna, Tenerife, Spain

⁴Departamento de Astrofísica, Universidad de La Laguna (ULL), E-38206 La Laguna, Tenerife, Spain

⁵Jodrell Bank Centre for Astrophysics, Alan Turing Building, Department of Physics and Astronomy, School of Natural Sciences, The University of Manchester, Oxford Road, Manchester, M13 9PL, UK

⁶Institut d'Astrophysique Spatiale, Université Paris-Sud / Paris-Saclay, 91405 Orsay Cedex, France

⁷Phase2 Microwave Ltd., Unit 1a, Boulton Rd, Pin Green Ind. Est., Stevenage, SG1 4QX, UK

⁸Department of Physics & Astronomy, University College London, Gower Place, London WC1E 6BT, UK

⁹Unidade Acadêmica de Física, Universidade Federal de Campina Grande, Campina Grande, PB, Brazil

¹⁰School of Physics and Astronomy, Cardiff University, Cardiff, CF10 3AT, UK

¹¹Instituto de Física, Universidade de Brasília, Brasília, DF, Brasil

¹²Center for Gravitation and Cosmology, YangZhou University, Yangzhou 225009, China

a full-sized prototype horn has been assembled. It has an average insertion loss of around 0.15 dB across the band, with a return loss around -25 dB. The main beam is Gaussian with the first sidelobe at around -25 dB. A septum polariser to separate the signal into the two hands of circular polarization has also been designed, built and tested.

Keywords Radio astronomy · radio telescope · corrugated feed horn · polariser

1 Introduction

The Baryon Acoustic Oscillations (BAOs) from Integrated Neutral Gas Observations (BINGO) telescope [1, 2, 3, 4, 5] will observe integrated HI signals in the redshift range $z = 0.13$ – 0.48 to constrain the properties of the Dark Sector [6]. It uses the concept of “single dish, many horns”, with a pair of 40-m mirrors and approximately 50 horns in a compact range layout to observe the redshifted 1420 MHz HI line emission at frequencies of 980–1260 MHz. Using the HI emission line as a proxy for total matter observation, the BINGO telescope will probe the redshift range where dark energy becomes dominant. This will be complementary to other large-scale structure projects operating at optical or other radio frequencies.

Very clean optics with low sidelobes is a critical part of the telescope design to achieve the high contrast ratio between the bright foregrounds and the faint HI signals. This contrast will allow component separation techniques to work efficiently [7, 8, 9], as well as reduce sensitivity to sources of radio frequency interference [10]. A compact range layout (crossed-Dragone) meets these requirements, but it needs very large horns with apertures of around 2 m to provide the relatively small beamwidths necessary to appropriately illuminate the secondary mirror. These horns also need to have very low sidelobes to reduce ground pickup.

Manufacturing smooth-sided large horns with narrow bandwidths is relatively simple. Illustrative cases are the horns being used for military radars and the horn used in Bell Labs for the discovery of the Cosmic Microwave Background Radiation [11]. However, a corrugated horn is needed to cover the large frequency range while maintaining the beam performance needed for BINGO. These are common for small to medium-sized horns (e.g., [12, 13]), but not for the >1 m-diameter required for BINGO, leading to the novel construction approach described below.

An exception is the L-band horn for EVLA [14], produced by the National Radio Astronomy Observatory (NRAO) and briefly discussed at the end of Subsection 3.2. It has a comparable size at similar frequencies to BINGO, but has a different design and uses a slightly different method of fabrication.

In this paper we summarise the design, construction and testing of a BINGO prototype horn and polariser. Section 2 presents the requirements for the horn with the chosen optical design. Section 3 discusses the challenges

of constructing the large horn and the adopted solution. Sections 4 and Section 5 contains, respectively, the methods used for testing the horn and the polariser connected to it, and the results for both tests. In Section 7 we discuss future work and present our conclusions.

2 Requirements and optical design

The current optical design for BINGO has a focal length of 63 m. In order to slightly under-illuminate the secondary mirror, the horns need to have an aperture of around 2 m and it is this large size that presents a significant construction challenge. With slight under-illumination of the secondary, the resulting full width at half maximum (FWHM) for the whole telescope is $\sim 40'$, maintaining the original angular resolution proposed in [2]. The horns need to have very low sidelobes and the beam to be tapered so the illumination is more than -20 dB at the edge of the secondary mirror in order to minimize the spillover, and thus the ground pickup. The resulting very clean beam pattern is vital to enable the faint HI signal to be efficiently separated from the bright Galactic foreground emission, whose signal is about 4 orders of magnitude brighter than HI. Our adopted crossed-Dragone configuration has been a common choice for many Cosmic Microwave Background (CMB) experiments in the last 15 years (see, e.g., [15, 16, 17]).

Given the bandwidth of 980–1260 MHz, the design that best satisfies the above requirements across the whole band while having a low ellipticity, a low cross-polarisation and a low return loss, are corrugated horns. As they operate at room temperature, the insertion loss should be less than 0.1 dB across the band, which would limit the increase in the system temperature to around 7 K. To be well matched with the rest of the system, including the receiver, the horns should ideally have around -40 dB return loss across the band.

With such a large aperture setting the beamwidth of the horn, in order to limit its length for manufacturing purposes, we had to choose a profile allowing for a compact horn. Following a previous study [18] which led to a design adopted for previous instruments (QUIJOTE and QUBIC for instance, [19, 20]), a Winston-like corrugated horn design with a circular aperture has been adopted for BINGO. This profile led to a maximum diameter of 1725.9 mm and length of 4300 mm (shown in Fig. 2).

The design was optimised using the mode-matching software CORRUG (S.M.T Consultancies Ltd.)¹ to model the beam and return loss properties. The corrugations consist of a series of rings with a width (or thickness) of 3.4 cm, corresponding to $1/8$ of the wavelength of the central observing frequency of 1.1 GHz. The rings have alternating diameters (listed in Table 1), creating the corrugation depth (each set for top and bottom of the corrugations). The horn has been designed in order to reach an edge taper below -20 dB at 19° across the whole band (horn beam power at the edge of the

¹ <http://www.smtconsultancies.co.uk/products/corrug/corrug.php>

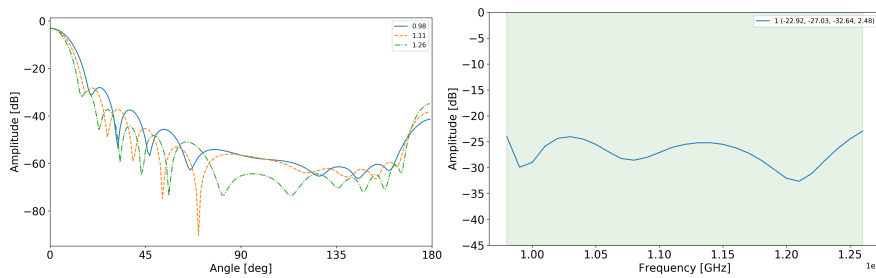


Fig. 1 Simulations of the beam pattern (left) and the return loss (right) of the BINGO horn design

secondary mirror of the telescope). Together with the low sidelobe level (below -27 dB for the first sidelobe), this results in a spillover below 2%.

Simulations of the beam pattern and return loss were then computed using the 3D Computer Simulation Technology (CST) package for a horn with the above ring diameters, and are shown in Figure 1. The predicted sidelobe performance is excellent with the far-out sidelobes at the -40 dB level. On the other hand, the predicted return loss, particularly at lower frequencies, is acceptable but less than ideal.

The radio emission from the Galaxy and extragalactic sources has a significant fraction of linear polarization. Moreover, the polarization position angle can be frequency-dependent due to Faraday rotation and as a consequence, the measured strength of a linear polarized signal can have an induced frequency dependence that might mimic that from redshifted hydrogen emission. To eliminate this problem it is desirable to make observations using circular polarization. For this reason a polariser is connected to the horn to receive the two hands of circular polarization. The design criteria were that the cross-polarization leakage across the band be less than -20 dB and the return loss be better than -25 dB.

3 Challenges of horn fabrication

The traditional method to manufacture corrugated horns for radio astronomy is to use a Computer Numerical Control (CNC) machine to manufacture it from a solid block of material. However, it is very expensive and not practical for the very large horns required for BINGO. Instead, the possibility of constructing them using alternative methods, including layered foam sheets and aluminum profiles bent to produce the corrugations were investigated.

3.1 Foam sheets

Earlier versions of the BINGO project explored the idea of using sheets of insulating foam. Such sheets are light, inexpensive, widely available and coated

Table 1 The diameters of each ring in the prototype horn

Ring (#)	Diameter (mm)						
1	1725.9	33	1555.2	65	1295.7	97	829.5
2	1581	34	1406.2	66	1138.9	98	648.3
3	1717	35	1542.2	67	1274.9	99	784.3
4	1571.9	36	1392.8	68	1117.3	100	599.2
5	1707.9	37	1528.8	69	1253.3	101	735.2
6	1562.6	38	1379	70	1095	102	545.4
7	1698.6	39	1515	71	1231	103	681.4
8	1553.1	40	1364.9	72	1071.8	104	485.7
9	1689.1	41	1500.9	73	1207.8	105	621.7
10	1553.1	42	1350.4	74	1047.7	106	418.2
11	1679.4	43	1486.4	75	1183.7	107	554.2
12	1553.4	44	1335.5	76	1022.6	108	339.7
13	1669.4	45	1471.5	77	1158.6	109	475.7
14	1523.2	46	1320.1	78	996.5	110	244.1
15	1659.2	47	1456.1	79	1132.5	111	402.2
16	1512.7	48	1304.4	80	969.2	112	197
17	1648.7	49	1440.4	81	1105.2	113	382
18	1502	50	1288.2	82	940.7	114	194
19	1638	51	1424.1	83	1076.7	115	380.6
20	1491	52	1271.4	84	910.9	116	197
21	1627	53	1407.4	85	1046.9	117	422.6
22	1479.8	54	1254.2	86	879.6	118	197
23	1615.8	55	1390.2	87	1015.6	119	386
24	1468.3	56	1236.5	88	846.6	120	197
25	1604.3	57	1372.5	89	982.6	121	410.6
26	1456.5	58	1218.2	90	811.8	122	197
27	1592.5	59	1354.2	91	947.8	123	424
28	1444.4	60	1199.3	92	774.8	124	197
29	1580.4	61	1335.3	93	910.8	125	483.2
30	1432	62	1179.9	94	735.6	126	197
31	1568	63	1315.9	95	871.6	127	466.2
32	1419.2	64	1159.7	96	693.5	128	197

with a thin layer of aluminum foil. Holes of the appropriate diameter could be cut into each sheet and the exposed edges covered with copper or aluminum tape to provide a continuous internal conducting surface. Initial tests with a horn of diameter 0.55 m made up of 78 of these sheets gave excellent results, with insertion loss around 0.1 dB. Unfortunately scaling up to a diameter of around 1 m was not so successful: similar performance levels could be achieved for short periods but not reliably maintained from day to day. Additionally, such sheets are likely not the best choice to perform under the high temperatures (year average of 26°C) on site during the full mission. The findings above led to the search of an alternative approach.

3.2 Aluminum profiles

One of the alternative construction approaches investigated, and which was considered the most promising in terms of costs and delivering a lightweight

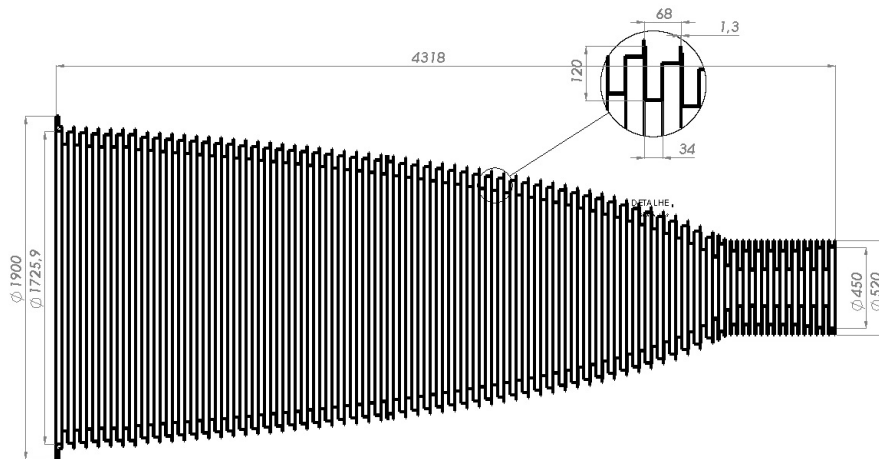


Fig. 2 Engineering drawing for the horn. The insert contains the “upside-down chair” profile used to produce the desired corrugation



Fig. 3 Left: horn cut, with the mounting right to the left. Right: Opposite view, with mounting point in the machined ring in the middle of the horn

unit, is to bend relatively thin chair-shaped sections (see Figure 2) of aluminum into circles of appropriate diameter and then join them together. This technique was used to produce all the larger diameter rings for a corrugated horn prototype, except for the largest one, which was manufactured using CNC machines for rigidity. The throat section of the horn was made using annuli cut from aluminum sheets, with a sheet of aluminum bent around to form the centre of the horn ring, welded together to make a ring. The centre mounting ring, and the last throat ring, were made with a CNC machine, again for rigidity (see Figure 3). The rings were joined together either by welding, riveting or bolting depending on ring diameter. A structural analysis was conducted in parallel with prototype fabrication and will be described in Sec. 3.3.



Fig. 4 The horn construction process. Starting from chair-shaped profiles bent out of a single sheet of aluminum (top-left), these profiles are then bent into rings. Top-middle: View of the 3 rollers used for conformation. Top-right: Side view of the fitting of the profile onto the rollers. Before being welded together to produce a complete ring (bottom-left) and any deviations smoothed out (bottom-middle). They are then stacked and riveted to each other (bottom-right) to form the complete horn

Preliminary studies indicated that two families of aluminum alloys (5000 and 6000) might have the required properties to be formed into the shaped profile. A high level of malleability of the aluminum alloy used for fabrication was required to withstand cold mechanical conformation without weakening the material, particularly for the smaller radius profiles. Also relevant is the hardness of the material, the thickness and internal radii of the profile. This is important in order to allow the bending of the rings without causing undesirable deformation stress at those edges and the ease at which it can be welded to close the rings while minimising the deformations in the bent profile. The chosen alloy was Al5052 and, based on the properties of this material, an appropriate tool to extrude the profiles could be designed.

Calfer², a spin-off company from the Brazilian airplane manufacturing industry, was contacted to produce a prototype horn. This included the manufacturing of the proper tool to bend the profiles into shape according to the required dimensions and tolerances. The profiles are shown in Figure 4 (top-left). The chair-shaped material with these profiles was then fed through a bending machine using rollers that were specially designed to accommodate the profile (Figure 4, top-middle and top-right). Due to the size and tolerances (better than 1 mm deviation from designed ring dimensions) required by the BINGO design, it is essential that small deformations, usual in the bending process, are minimized at the bending and welding stages, reducing finishing time and final costs.

A single bending tool with three wheels can be adjusted to make rings with a range of diameters. The end of the rings are welded together, making use of a rigid template for proper positioning (Figure 4, bottom-left). Heating

² <http://calfer.com.br/>

of the material during the welding slightly deforms the nearby areas, thus requiring some rework before assembling the rings (Figure 4, bottom-middle and bottom-right).

Before assembling the parts, there must be a careful dimensional and visual inspection of each ring, since access to the interior of the horn is difficult after the completion of the assembly process. The inner surface finish of each ring plays an important role in the final performance of the horn. The rings should not have significant irregularities on their surfaces and were sanded to a smooth finish. The dimensions were checked on a gauge table after the welding process.

The final assembly of the rings to form the horn was done manually. The best alignment of the center of all rings was achieved after careful calibration of the diameters. This ring alignment operation is extremely important because it can directly influence the electromagnetic performance. Two of the rings, one at the aperture of the horn and one in the middle, were reinforced to act as a rigid structure to receive lift lugs for maneuvering the horn after assembly. The prototype manufactured in this way has a total mass of about 448 kg (including bolts and lift lugs) with a build accuracy equal to or better than 1.0 mm on average.

For the NRAO E-VLA project a L-band horn of slightly smaller than the BINGO horn (4.1 m length; 1.5 m aperture diameter) was designed. The horns were made by stacking aluminum components (rings and bands made of separate aluminum alloys) and holding them together with a fiberglass shell on the outside [21], [22]. The aluminum alloy used is very similar to the one adopted in this work (6061 and 5052 for the NRAO E-VLA versus 5052 only, for the BINGO rings). The assembly process is described in [14], and consists of setting up pre-produced corrugations in an assembly fixture provided by NRAO. These corrugations are a mix of fully machined rings and rings made by a combination of sheet metal disks and bands, which also work as flanges to assemble different sections of the horn. The estimated delivery schedule for the NRAO horns is a minimum of 6, maximum of 10 units per year, after the contractor has all needed components, which is around half the rate expected for BINGO horn production (minimum of 12, maximum of 20 horns per year). The higher delivery rate is important for BINGO in order to construct the full array of around 50 horns along with the telescope over a three-year period.

3.3 Structural Analysis

In order to guarantee that the mechanical structure of the horn would support its own weight, an engineering company (Analysis Engenharia e Consultoria Ltda., based in S. José dos Campos) was hired to perform a structural analysis of the mechanical design. The NASTRAN finite element program was used in the analysis and the horn model contained 587 098 elements, 533 520 nodes and a full mass of 448 kg, and considered the extreme situation of the horn attached to a fixed structure by the largest horn ring only.

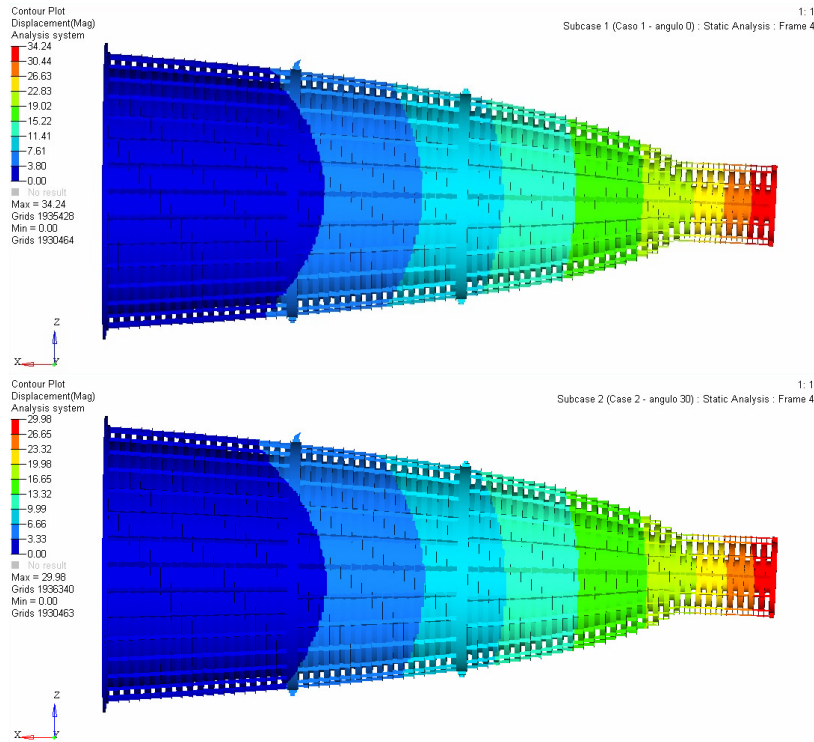


Fig. 5 Top: Deformation of the horn under its own weight, for a horizontal anchoring through its aperture at 0° . Bottom: Same as above, for an anchoring through its aperture at 30° from horizontal

The analysis reported the maximum elastic deformations of the structure according to the force loads F_x , F_y and F_z and the tension distributed over the horn structure, in four sectors: near the horn aperture, near the center of mass (to the larger diameters), near the center of mass (close to the throat) and near the throat, including the throat itself. Both were computed considering deformations caused by gravity action and external wind load (assumed blowing perpendicular to the horn surface, parallel to the horizontal and perpendicular to the gravity force vector). The full analysis is presented in [23].

An example case explored in the analysis is presented in Figure 5. The main results indicate that deformation and tension under gravity is not a major issue for the horn, but might be an issue if the horn is in the open and exposed to high winds. A summary of values for all cases are presented in Table 2. Displacements (column 2) are measured compared to a null displacement in the direction perpendicular to the optical axis (for gravity). The angular displacement corresponds to the linear displacement. The displacement caused by wind plus weight is also in the direction perpendicular to the optical axis of the horn. The maximum tension along the horn axis, around the rings, are computed after the estimated deformations. Maximum tensions are always

Table 2 Horn Structural Analysis - Summary of deformation cases

Description	Displacement (mm)	Angular displacement (°)	Maximum Tension intensity (MPa)	Safety Margin %
Weight only (0° from horizontal)	34.2	0.45	72.0	226
Weight only (+30° from horizontal)	30.0	0.40	68.8	241
Weight and wind (0° from horizontal)	85.4	1.13	213.2	10
Weight and wind (+30° from horizontal)	85.0	1.13	198.4	18

located closer to the aperture and distributed along the superior surface of the horn. The safety margin (MS) is computed after the maximum tension, according to [23]:

$$MS_{\text{yield}} = \frac{F_{\text{ty}}}{F_{\text{max}} * \text{FS}} - 1, \quad (1)$$

where f_{max} is the maximum stress calculated according to the Von Mises conditions, F_{ty} is the flow limit and FS is the safety factor is chosen as 15% (meaning 15% larger than F_{max}). Column 4 (Safety Margin) indicates that the safety margin for a given tension allows deformations which are 226%, 241%, 10% and 18%. We do not expect this to be a significant issue because the engineering solution for the focal plane assemblage is to fix each horn in an hexagonal aluminum structure that will provide the necessary rigidity and, additionally, shield each of these structures from the weather.

4 Horn tests

There are three main radio frequency test procedures required to characterise the performance of a horn. The first is to measure the insertion loss, i.e., the loss of the signal as it passes through the device. The second is to measure the return loss, i.e., how much signal is reflected by the horn due to small impedance mismatches. The third is the characterization of the beam. These need to be measured across the frequency range over which the horn is required to operate.

4.1 Insertion and return loss

Insertion and return loss measurements of the horn were made using a Vector Network Analyser (VNA) to transmit a signal and record the returned signal (the “S11” parameter). For the insertion loss, a metal reflector was placed at the end of the horn so that the returned signal has passed through the horn twice (and consequently, the measured S11 parameter needs to be divided by two to calculate the insertion loss). An ideal horn should have zero insertion loss. For the return loss, an absorbing screen covering the whole aperture of the



Fig. 6 Left: Initial horn testing at Calfer. Middle: Testing the horn at INPE with a aluminum plate covering the horn aperture. Right: At INPE with Eccosorb covering the horn aperture

horn (trade name Eccosorb) was used to absorb the transmitted signal, while the VNA measures that part of the signal reflected within the horn structure. Figure 6 (mid- and right-panels) show the horn with a metal reflector and eccosorb in place.

Circular-to-rectangular and rectangular-to-coax transitions were manufactured at Calfer and Phase2 Microwave, respectively. The rectangular-to-coax transition has internal dimensions of 97.79×195.58 mm and the circular-to-rectangular transition consists in three units, starting with a circular-to-rectangular transition that couples to two subsequent units towards a rectangular transition to be coupled to the rectangular-to-coax waveguide. The WG5 to coax drawings can be seen in Figure 7. The insertion loss of the coax-to-WG5 transition was measured with the VNA, and we obtained losses between -0.025 and -0.12 dB (mean of -0.075 dB) in the BINGO band. The measured rectangular-to-circular insertion loss figures were between -0.06 and -0.15 dB (mean of -0.1 dB).

Input and return loss measurements can easily be affected by errors in the VNA calibration. In particular, any losses in the connecting cables and waveguide transitions connected to the horns need to be measured and calibrated out to give just the horn properties. Initial measurements made use of standard VNA calibration components at the end of the SMA cables, and the loss of the waveguide components except for the horn has to be subtracted from the measurements later on. Once this was done the actual horn return and insertion loss were measured. Subsequently, a $1/8$ wavelength waveguide offset and a short (rectangular blanking plate) were manufactured and used to perform “waveguide calibration” including the waveguide to coax transition. This method is to be preferred when measuring waveguide components, however, this calibration does not include the rectangular-to-circular transi-

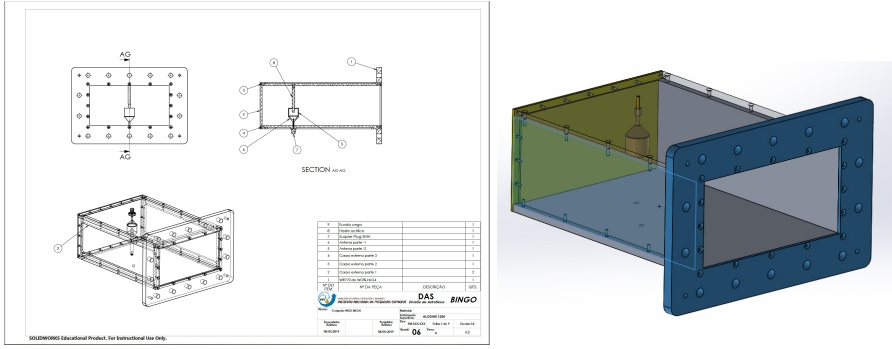


Fig. 7 Left: WG5 transition, with the internal antenna and external connector. Right: WG5 transition, 3D (transparent) view

tion. All measurements were made with an Agilent N5230C PNA-L desktop Network Analyser.

Initial measurements of the insertion loss of the horn were made at Calfer (Figure 6, left panel) to check that the horn was functioning correctly before acceptance. These were followed by more intensive tests during 2018 of both the insertion and return loss at INPE, using cable calibration. The final set of measurements presented here were taken in February and March 2019 and used waveguide calibration.

The final insertion loss measurement of the horn and circular-to-rectangular transition is shown in Figure 8. It will be noted that there are regular spikes in the insertion loss, which arise from standing waves in the formed “cavity” between the reflecting plate and some part of the horn throat. These spikes will not be present in normal operation without the reflecting plate and can be ignored. If we do this the measured loss within the BINGO band is 0.14 dB, with a standard deviation of 0.05 dB. We estimate the uncertainty on this measurement due to VNA calibration to be around 0.05 dB. This loss would result in an increase in system temperature of around 10 K. We have identified areas in which small modifications in the fabrication process can be made to try and reduce this loss, and these will be tested with a second prototype.

4.2 Beam measurements

The Laboratory of Integration and Tests (LIT) is a Brazilian facility to integrate and test satellites up to the 2-ton class, located at INPE, in São José dos Campos, Brazil. It has a far-field antenna test range that was used to measure the horn beam pattern. Measurements of the prototype BINGO horn were conducted during 22–25 May 2018.

The test facility consists of a 9 m wide \times 9 m tall \times 10 m deep chamber, fully covered inside with absorbing cones and facing the transmitting antenna through a 9 m \times 9 m open window. The transmitter is located 80 m away from the mounting system and produces polarized horizontal and vertical signals.

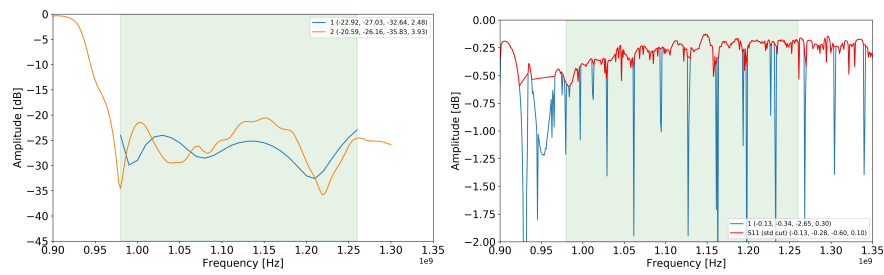


Fig. 8 Left: The return loss of the prototype horn. Right: The insertion loss of the prototype horn, with waveguide calibration. The measurement is of both the circular-to-rectangular transition and the horn, with the reflector at the end, so the two passes double the values. The raw measurement is shown in green, after spike removal is shown in red. The numbers in the legend are the maximum, mean, minimum and standard deviation within the BINGO band of 980–1260MHz (shown by the green shaded region)

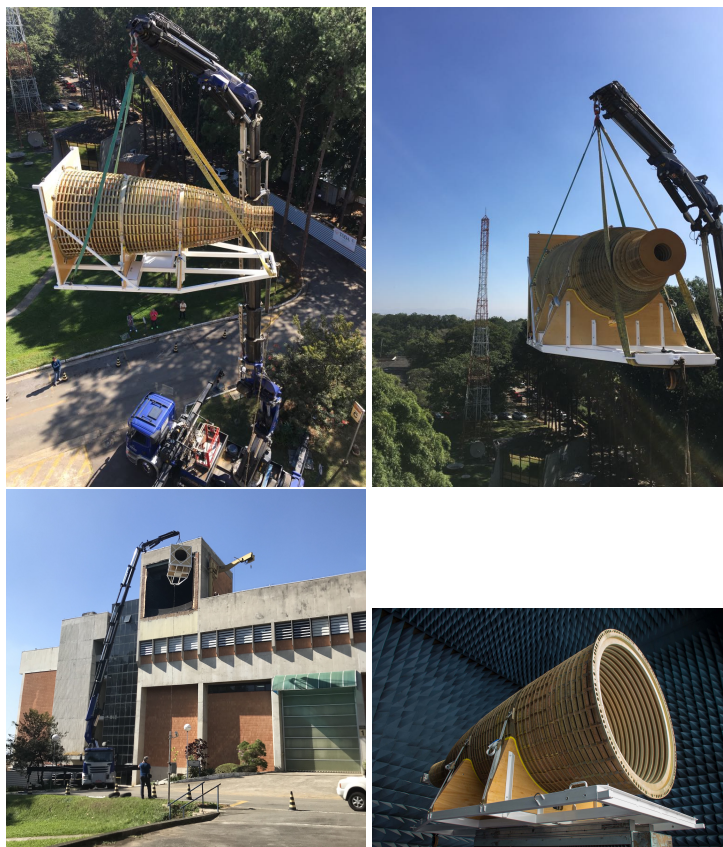


Fig. 9 Top: Horn being suspended, with its cart, to the opening of the anechoic chamber. Bottom right: The horn mounted in the LIT test facility

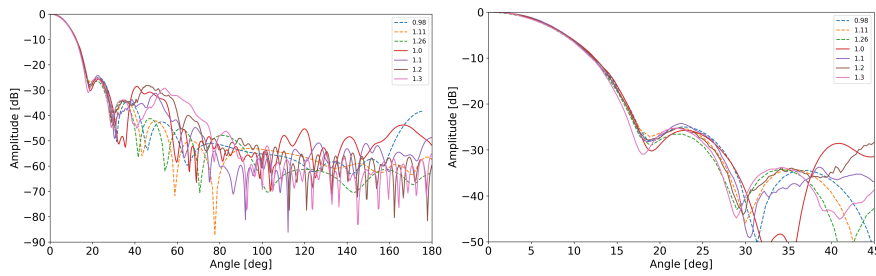


Fig. 10 The beam patterns at a range of frequencies across the BINGO band, rescaled in width to 1 GHz and in amplitude to a maximum of 0 dB. Left: full azimuth range. Right: a zoom-in on the first two sidelobes. The first sidelobe is around 25 dB lower than the main beam

The horn under test in the chamber is mounted on top of a pivoting system with the horn aperture located about 1.5 m ahead of the rotation axis. This system is capable of continuous 360° horizontal rotation, clock and counter-clockwise, and the horn response to the signal emitted by the far-field transmitted is continuously measured until a full horizontal rotation is completed. Chamber temperature and humidity were not controlled nor taken into account during the data acquisition process, but should not have a significant effect on these measurements.

The radiation pattern measurements were performed using linear polarization transmitters on the tower, with 17 measurements at 25 MHz intervals from 900 to 1300 MHz. The signal was generated by a ANRITSU MG3649B equipment. The horn was connected to a MI-1797 receiver (fabricated by Scientific Devices Australia Pty. Ltd. - SDA) via the same circular-to-rectangular and rectangular-to-coax transitions as described in the previous section and the acquisition software is also from SDA. Each frequency was measured in both vertical and horizontal polarization. The directivity was calculated by numerically integrating the irradiation diagrams. Table 3 shows a sample of the data. Directivity and FWHM are essentially the same for both polarizations in each frequency, indicating that the beams should be nearly circular across the frequency band.

The front to back response differences show different values for vertical and horizontal polarization, with a spread of about 25 dB in the horizontal polarization and 15 dB in the vertical polarization. Nevertheless, the worst case (for horizontal polarization at 900 MHz) is 46 dB, and, inside the nominal band (980–1260 MHz), the worst response is 48.39 dB, also for horizontal polarization.

Minimum rejection refers to the cross-polarization (leakage from V to H during H measurements and vice-versa) contamination and was measured at 900, 1000, 1050, 1100, 1150, 1200 and 1300 MHz. The worst case is a minimum rejection of 19.7 dB at 1150 MHz in the vertical polarization. Beam patterns are shown in Figure 10, with the performance along a full azimuth scan in the left-hand panel, and a zoom over 0–45° in the right-hand panel. On av-

Table 3 Beam measurements. Left: horizontal polarization. Right: vertical polarization. Minimum rejection was not measured at all frequencies

Freq (MHz)	Directivity (dB)	FWHM (deg)	Min. rejection (dB)	Front to back difference (dB)	Directivity (dB)	FWHM (deg)	Min. rejection (dB)	Front to back difference (dB)
950	22.4	14.6	–	47.0	22.7	13.4	–	56.2
1000	23.1	13.8	22.5	51.7	23.0	13.5	20.5	64.7
1050	23.5	13.1	28.2	54.2	23.5	12.9	35.9	57.2
1100	23.9	12.4	25.6	58.2	23.9	12.4	30.5	56.2
1150	24.3	11.8	20.0	72.8	24.4	11.7	19.7	55.4
1200	24.7	11.1	26.4	57.2	24.6	11.1	26.0	63.6
1250	25.2	10.3	–	56.1	24.9	10.6	–	57.1

erage, the response of the first sidelobe is 25 dB lower than the main lobe, in agreement with the simulations. These levels of beam sidelobes are similar to those obtained by the VLA L-band horn. The simulated beam pattern in Figure 1 is better than the measured one by about 5 dB in the second sidelobe, which may be due to the horn support structure, and as such we are looking for improvement areas in this specific parameter of the horn and the support structure for the second prototype.

5 Polariser

As described in Section 2, it is desirable to make observations using circular polarisation. In this section we describe the transition required to connect the circular horn throat to the square input to the polariser, followed by a description of the polarization design itself. Finally, laboratory measurements of the performance are presented.

5.1 The circular to square transition

The termination of the horn is circular but the input to the polariser is a square waveguide so a transition is required. Initially a transformer that gradually merged the circular to square profile was evaluated but in the end, a two-step design was found to give superior performance with a shorter overall length. The total length was under 200 mm. The design and the predicted return loss is shown in Figure 11. The return loss should be better than -30 dB across the band of interest.

5.2 Polariser design

The polariser was designed in the UK by Phase 2 Microwave and manufactured in Brazil by Metalcard. The polariser needs to be able to take the two incoming hands of circular polarization from the horn and convert them to linear with high isolation between them. The output should be in a rectangular guide because the next component in the receiver chain is a waveguide magic-tee.

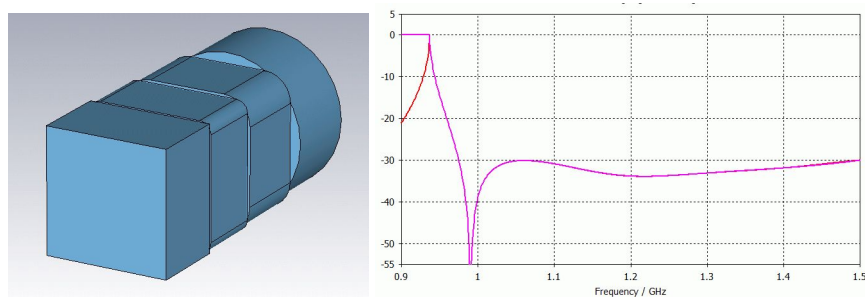


Fig. 11 Left: Schematic circular-to-square transition design. Right: The predicted return loss of the transition

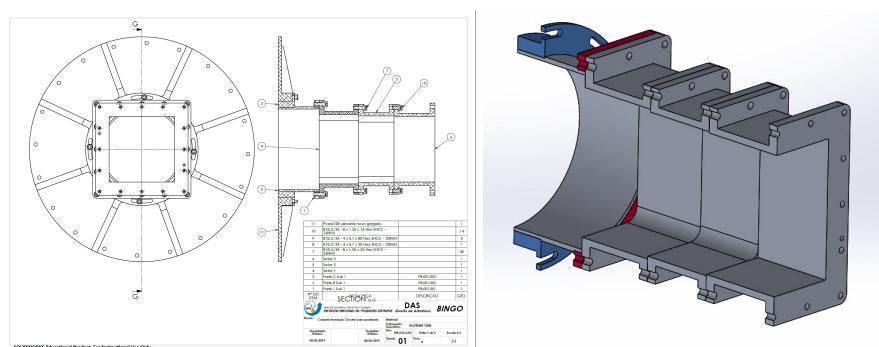


Fig. 12 Left: Rectangular to square transition (front view) drawing, used to attach to a rectangular transition. Right: Rectangular to square transition, exploded view

While specialised waveguide sizes could be used it was decided to make the output in waveguide WG5 (WR770) to simplify connection to the magic-tee and to allow for the use of standard test equipment. Figure 13 shows the 3D rendering of the design.

The relative bandwidth is moderately high at 25% and the use of a stepped septum polariser is the normal solution for this sort of bandwidth. Since a circular guide version has a narrower bandwidth than the square guide version, the latter was adopted. Also, designs in the square guide were already available at higher frequencies so these could be adapted. The disadvantage is that a circular to square transformer is required as discussed above. The idea of a septum polariser design was originally published in [24].

A septum with four steps was chosen after a five-step septum was investigated but showed no real benefit in performance. Analytical design is not available so software optimisation of the septum step lengths was required. The design consists of four parts. The septum polariser is followed by a “joggle” to separate the output waveguides and two transitions from the special waveguide size to standard WG5. Preceding the septum is a phasing section. The dimension of the square guide was chosen to be 160 mm. For this, the H01 cutoff is 936 MHz, i.e., not too near the 980 MHz at the bottom of the

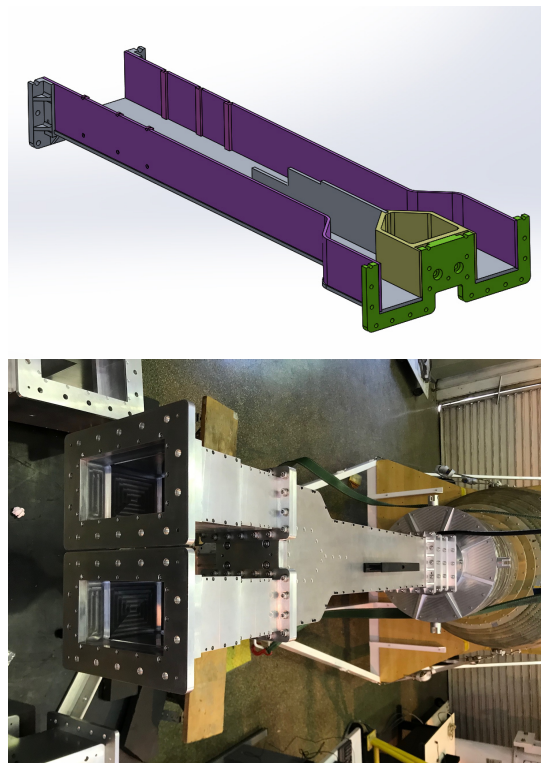


Fig. 13 Left: 3D rendering of the internal part of the polariser, showing the septum in detail. Right: Rear view of the transitions, polariser and the horn

BINGO band. The next modes are the H₁₁/E₁₁ modes at 1.36 GHz. The mode matching Microwave Wizard (from Mician) software was used to optimise the design. The predicted return loss over the band is better than 20 dB with 25 dB isolation between orthogonal polarizations. Figure 13 shows the manufactured hardware.

To form a pure circular wave we need two linear waves at exactly 90 degrees to each other. It was found that this was very difficult to achieve at the top end of the band and in the end, three pairs of irises, parallel to the septum were used between the septum and the horn which allowed the phase to be improved by 5 degrees to be within -6 to $+2.5$ degrees across the required band.

5.3 Performance testing

Measurement of a polariser is difficult and several setups are typically needed to capture all the information. We did not have the benefit of having any

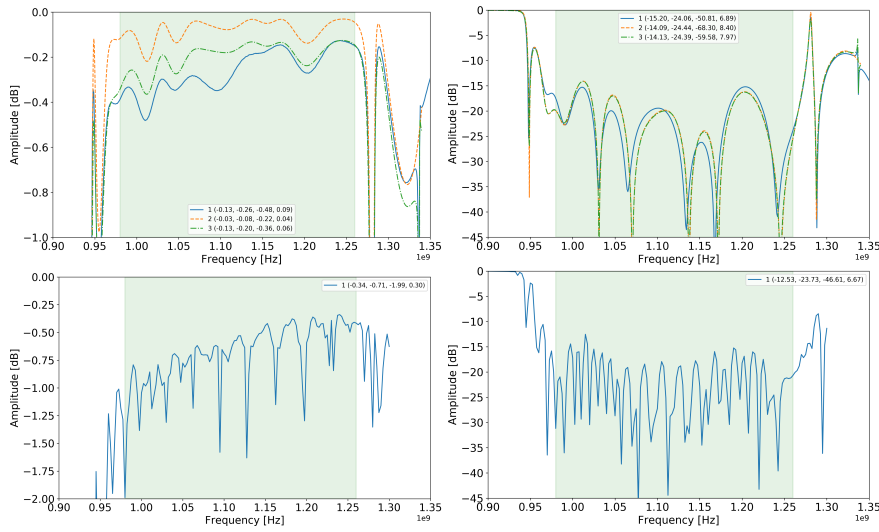


Fig. 14 Top: Measurement of the polariser only; the solid blue line is the measurement, while the orange and green dashed lines show simulations with different levels of loss. Left: insertion loss. Right: return loss. Bottom: measurements of the polariser mounted on the horn. Left: insertion loss. Right: return loss

waveguide loads, which further restricted the possibilities. One good method of testing is to put two polarisers back to back but again, because of the size and cost, only one polariser was available for testing. We used a short on the square waveguide output and compare the response measured with the VNA with the simulated response. The measurements were done in the lab at INPE and generally showed good agreement with theory, giving high confidence that the design was realised as expected. The most noticeable deviation was the insertion loss which was higher than desired, at 0.12 dB on average across the band (Figure 14). We have identified places where fixing the different parts of the polariser together can be improved and it is expected that by doing this we will be able to reduce the loss in subsequent examples.

The combined insertion loss of the horn and polariser were also measured, and are shown in Figure 14. The average insertion loss across the band is 0.35 dB, with a standard deviation of 0.3 dB, without removing the spikes caused by standing waves. The return loss is -24 dB on average across the band.

6 Summary

The return and insertion losses for horn, polariser and transitions call tests are summarised in Table 4. Altogether, the performance of this first horn plus the front-end prototype should add approximately 20 K to BINGO noise budget. The beam response was summarized in Table 3. In addition, within

the frequency range 980–1260 MHz (nominal band) the horn has the following parameters:

1. Horn directivity varies from 22.7 dB to 25.3 dB;
2. The difference in FWHM for both polarizations is at most 0.31° at 1 GHz, remaining under 0.25° degrees everywhere else;
3. The front to back lobe rejection changes within the nominal band. The Worst measurements are 48.39 dB at 1 GHz (horizontal polarization) and 51.92 dB at 975 MHz (vertical polarization);
4. The minimum rejection for both polarizations is around 19.8 dB at 1150 MHz.
5. The first sidelobes are located within 20° – 30° and have amplitudes -25 dB lower than the main lobe.

Table 4 Horn measurements - summary

Unit	Insertion loss		Return loss	
	measured	predicted	measured	predicted
Horn	-0.14	-	-26.50	-28
Polariser	-0.12	-0.08	-24.06	-24.44
WG5 to coax	-0.075	-	< -30	-

7 Conclusions and future work

We have successfully built a large prototype corrugated horn for the BINGO telescope, which achieves low insertion loss (around 0.15 dB), good return loss (lower than -20 dB within the band), and with a clean beam with low sidelobes (lower than -27 dB within the band). The prototype horn will undergo further testing, including use for early astronomical observations at the BINGO site.

A second prototype is under construction, with improvements made to the construction process, such as the addition of a fourth roller to the bending machine, modified aluminium profiles with reinforced corners to reduce tearing during bending. These fabrication adjustments are intended to reduce the amount of human intervention involved in the horn production, which is a major contribution to the final cost when we proceed to the production of the full batch of around 50 horns in the near future. In addition to the mechanical improvements, refinements in the construction of both the horn and the polariser in order to improve the electromagnetic performance are being analysed for possible implementation in the fabrication of the upcoming units.

Acknowledgements We thank Jeff Peterson for useful conversations about the horn testing and to Martin Bluck for careful reading of the text. BINGO is funded by FAPESP (São Paulo State Agency for Research Support) through project 2014/07885-0. C.A.W. acknowledges support from CNPq through grant 313597/2014-6 and support from LIT Antenna Testing Facility. M.P. acknowledges funding from a FAPESP Young Investigator fellowship, grant 2015/19936-1. E.A. wishes to thank FAPESP and CNPq for several grants. V. L. acknowledges the postdoctoral FAPESP grant 2018/02026-0. E. M. acknowledges a

Ph.D. CAPES fellowship. F. V. acknowledges a CAPES M.Sc. fellowship. T.V. acknowledges CNPq Grant 308876/2014-8. Data reduction was performed using Python and the MATPLOTLIB, NUMPY and SCIPY packages.

Conflict of interest

The authors declare that they have no conflicts of interest.

References

1. R.A. Battye, M.L. Brown, I.W.A. Browne, R.J. Davis, P. Dewdney, C. Dickinson, G. Heron, B. Maffei, A. Pourtsidou, P.N. Wilkinson, *Proceedings of Moriond Cosmology* (2012)
2. R.A. Battye, I.W.A. Browne, C. Dickinson, G. Heron, B. Maffei, A. Pourtsidou, *Mon. Not. R. Astron. Soc.* **434**, 1239 (2013). DOI 10.1093/mnras/stt1082
3. R. Battye, I. Browne, T. Chen, C. Dickinson, S. Harper, L. Olivari, M. Peel, M. Remazeilles, S. Roychowdhury, P. Wilkinson, E. Abdalla, R. Abramo, E. Ferreira, A. Wuensche, T. Vilella, M. Caldas, G. Tancredi, A. Refregier, C. Monstein, F. Abdalla, A. Pourtsidou, B. Maffei, G. Pisano, Y.Z. Ma, *Proceedings of Recontres de Moriond* (2016)
4. C. Dickinson, *Proceedings of Moriond Cosmology* (2014)
5. C.A. Wuensche, B. Collaboration, *Journal of Physics: Conference Series* **1269**, Conference 1 (2019)
6. B. Wang, E. Abdalla, F. Atrio-Barandela, D. Pavon, *Rep. Prog. Phys.* **79**(9), 096901 (2016). DOI 10.1088/0034-4885/79/9/096901
7. M.A. Bigot-Sazy, C. Dickinson, R.A. Battye, I.W.A. Browne, Y.Z. Ma, B. Maffei, F. Noviello, M. Remazeilles, P.N. Wilkinson, *Mon. Not. R. Astron. Soc.* **454**, 3240 (2015). DOI 10.1093/mnras/stv2153
8. L.C. Olivari, M. Remazeilles, C. Dickinson, *Mon. Not. R. Astron. Soc.* **456**, 2749 (2016). DOI 10.1093/mnras/stv2884
9. L.C. Olivari, C. Dickinson, R.A. Battye, Y.Z. Ma, A.A. Costa, M. Remazeilles, S. Harper, *Mon. Not. R. Astron. Soc.* **473**, 4242 (2018). DOI 10.1093/mnras/stx2621
10. M.W. Peel, C.A. Wuensche, E. Abdalla, S. Antón, L. Barosi, I.W.A. Browne, M. Caldas, C. Dickinson, K.S.F. Fornazier, C. Monstein, C. Strauss, G. Tancredi, T. Vilella, *Journal of Astronomical Instrumentation* **8**(1), 1940005 (2019). DOI 10.1142/S2251171719400051
11. A.A. Penzias, R.W. Wilson, *Astrophys. J.* **142**, 419 (1965). DOI 10.1086/148307
12. C. Witebsky, G.F. Smoot, S. Levin, M. Bensadoun, *IEEE Transactions on Antennas and Propagation* **35**, 1310 (1987). DOI 10.1109/TAP.1987.1144021
13. J. Singal, D.J. Fixsen, A. Kogut, S. Levin, M. Limon, P. Lubin, P. Mirel, M. Seiffert, T. Vilella, E. Wollack, C.A. Wuensche, *Astrophys. J.* **730**, 138 (2011). DOI 10.1088/0004-637X/730/2/138
14. S. Srikanth, J. Ruff, E. Szpindor, Design, prototyping and measurement of evla l-band feed horn. Tech. rep., NRAO (2005). URL <https://library.nrao.edu/public/memos/evla/legacy/evlamemo87.pdf>
15. H. Tran, B. Johnson, M. Dragovan, J. Bock, A. Aljabri, A. Amblard, D. Bauman, M. Be-toule, T. Chui, L. Colombo, A. Cooray, D. Crumb, P. Day, C. Dickenson, D. Dowell, S. Golwala, K. Gorski, S. Hanany, W. Holmes, K. Irwin, B. Keating, C.L. Kuo, A. Lee, A. Lange, C. Lawrence, S. Meyer, N. Miller, H. Nguyen, E. Pierpaoli, N. Ponthieu, J.L. Puget, J. Raab, P. Richards, C. Satter, M. Seiffert, M. Shimon, B. Williams, J. Zmuidzinas, in *Space Telescopes and Instrumentation 2010: Optical, Infrared, and Millimeter Wave*, *Proc. of SPIE*, vol. 7731 (2010), *Proc. of SPIE*, vol. 7731, p. 77311R. DOI 10.1117/12.857423

16. J. Delabrouille, P. de Bernardis, F.R. Bouchet, A. Achúcarro, P.A.R. Ade, R. Allison, F. Arroja, E. Artal, M. Ashdown, C. Baccigalupi, M. Ballardini, A.J. Banday, R. Banerji, D. Barbosa, J. Bartlett, N. Bartolo, S. Basak, J.J.A. Baselmans, K. Basu, E.S. Battistelli, R. Battye, D. Baumann, A. Benoît, M. Bersanelli, A. Bideaud, M. Biesiada, M. Bilicki, A. Bonaldi, M. Bonato, J. Borrill, F. Boulanger, T. Brinckmann, M.L. Brown, M. Bucher, C. Burigana, A. Buzzelli, G. Cabass, Z.Y. Cai, M. Calvo, A. Caputo, C.S. Carvalho, F.J. Casas, G. Castellano, A. Catalano, A. Challinor, I. Charles, J. Chluba, D.L. Clements, S. Clesse, S. Colafrancesco, I. Colantoni, D. Contreras, A. Coppolecchia, M. Crook, G. D'Alessandro, G. D'Amico, A. da Silva, M. de Avillez, G. de Gasperis, M. De Petris, G. de Zotti, L. Danese, F.X. Désert, V. Desjacques, E. Di Valentino, C. Dickinson, J.M. Diego, S. Doyle, R. Durrer, C. Dvorkin, H.K. Eriksen, J. Errard, S. Feeney, R. Fernández-Cobos, F. Finelli, F. Forastieri, C. Franceschet, U. Fuskeland, S. Galli, R.T. Génova-Santos, M. Gerbino, E. Giusarma, A. Gomez, J. González-Nuevo, S. Grandis, J. Greenslade, J. Goupy, S. Hagstotz, S. Hanany, W. Handley, S. Henrot-Versillé, C. Hernández-Monteagudo, C. Hervias-Caimapo, M. Hills, M. Hindmarsh, E. Hivon, D.T. Hoang, D.C. Hooper, B. Hu, E. Keihänen, R. Keskitalo, K. Kiiveri, T. Kisner, T. Kitching, M. Kunz, H. Kurki-Suonio, G. Lagache, L. Lamagna, A. Lapi, A. Lasenby, M. Lattanzi, A.M.C. Le Brun, J. Lesgourgues, M. Liguori, V. Lindholm, J. Lizarraga, G. Luzzi, J.F. Macias-Perez, B. Maffei, N. Mandolesi, S. Martin, E. Martinez-Gonzalez, C.J.A.P. Martins, S. Masi, M. Massardi, S. Matarrese, P. Mazzotta, D. McCarthy, A. Melchiorri, J.B. Melin, A. Mennella, J. Mohr, D. Molinari, A. Monfardini, L. Montier, P. Natoli, M. Negrello, A. Notari, F. Noviello, F. Oppizzi, C. O'Sullivan, L. Pagano, A. Paiella, E. Pajer, D. Paoletti, S. Paradiso, R.B. Partridge, G. Patanchon, S.P. Patil, O. Perdereau, F. Piacentini, M. Piat, G. Pisano, L. Polastri, G. Polenta, A. Pollo, N. Ponthieu, V. Poulin, D. Prêle, M. Quartin, A. Ravenni, M. Remazeilles, A. Renzi, C. Ringeval, D. Roest, M. Roman, B.F. Roukema, J.A. Rubiño-Martin, L. Salvati, D. Scott, S. Serjeant, G. Signorelli, A.A. Starobinsky, R. Sunyaev, C.Y. Tan, A. Tartari, G. Tasinato, L. Toffolatti, M. Tomasi, J. Torrado, D. Tramonte, N. Trappe, S. Triqueneaux, M. Tristram, T. Trombetti, M. Tucci, C. Tucker, J. Urrestilla, J. Väliiviita, R. Van de Weygaert, B. Van Tent, V. Vennin, L. Verde, G. Vermeulen, P. Vielva, N. Vittorio, F. Voisin, C. Wallis, B. Wandelt, I.K. Wehus, J. Weller, K. Young, M. Zannoni, *J. Comp. Astrop. Phys.* **2018**(4), 014 (2018). DOI 10.1088/1475-7516/2018/04/014
17. S. Kashima, M. Hazumi, H. Imada, N. Katayama, T. Matsumura, Y. Sekimoto, H. Sugai, *Appl. Optics* **57**(15), 4171 (2018). DOI 10.1364/AO.57.004171
18. B. Maffei, E. Gleeson, J.A. Murphy, G. Pisano, *Proc. SPIE 5498, Millimeter and Submillimeter Detectors for Astronomy II* **5498** (2004). DOI 10.1117/12.552922. URL <https://doi.org/10.1117/12.552922>
19. R.J. Hoyland, M. Aguiar-González, B. Aja, J. Ariño, E. Artal, R.B. Barreiro, E.J. Blackhurst, J. Cagigas, J.L. Cano de Diego, F.J. Casas, R.J. Davis, C. Dickinson, B.E. Arriaga, R. Fernandez-Cobos, L. de la Fuente, R. Génova-Santos, A. Gómez, C. Gomez, F. Gómez-Reñasco, K. Grainge, S. Harper, D. Herran, J.M. Herreros, G.A. Herrera, M.P. Hobson, A.N. Lasenby, M. Lopez-Caniego, C. López-Caraballo, B. Maffei, E. Martinez-Gonzalez, M. McCulloch, S. Melhuish, A. Mediavilla, G. Murga, D. Ortiz, L. Piccirillo, G. Pisano, R. Rebolo-López, J.A. Rubiño-Martin, J.L. Ruiz, V. Sanchez de la Rosa, R. Sanquircé, A. Vega-Moreno, P. Vielva, T. Viera-Curbelo, E. Villa, A. Vizcargüenaga, R.A. Watson, in *Millimeter, Submillimeter, and Far-Infrared Detectors and Instrumentation for Astronomy VI, Proc. of SPIE*, vol. 8452 (2012), *Proc. of SPIE*, vol. 8452, p. 845233. DOI 10.1117/12.925349
20. J. Aumont, S. Banfi, P. Battaglia, E.S. Battistelli, A. Baù, B. Bélier, D. Bennett, L. Bergé, J.P. Bernard, M. Bersanelli, M.A. Bigot-Sazy, N. Bleurvacq, G. Bordier, J. Brossard, E.F. Bunn, D. Buzi, A. Buzzelli, D. Camilleri, F. Cavaliere, P. Chanial, C. Chapron, G. Coppi, A. Coppolecchia, F. Couchot, R. D'Agostino, G. D'Alessandro, P. de Bernardis, G. De Gasperis, M. De Petris, T. Decourcelle, F. Del Torto, L. Dumoulin, A. Etchegoyen, C. Franceschet, B. Garcia, A. Gault, D. Gayer, M. Gervasi, A. Ghribi, M. Giard, Y. Giraud-Héraud, M. Gradziel, L. Grandsire, J.C. Hamilton, D. Harari, V. Haynes, S. Henrot-Versillé, N. Holtzer, J. Kaplan, A. Korotkov, L. Lamagna, J. Lande, S. Loucatos, A. Lowitz, V. Lukovic, B. Maffei, S. Marnieros, J. Martino,

- S. Masi, A. May, M. McCulloch, M.C. Medina, S. Melhuish, A. Mennella, L. Montier, A. Murphy, D. Néel, M.W. Ng, C. O'Sullivan, A. Paiella, F. Pajot, A. Passerini, A. Pelosi, C. Perbost, O. Perdereau, F. Piacentini, M. Piat, L. Piccirillo, G. Pisano, D. Prêle, R. Puddu, D. Rambaud, O. Rigaut, G.E. Romero, M. Salatino, A. Schillaci, S. Scully, M. Stolpovskiy, F. Suarez, A. Tartari, P. Timbie, M. Tristram, G. Tucker, D. Viganò, N. Vittori, F. Voisin, B. Watson, M. Zannoni, A. Zullo, arXiv e-prints (2016)
21. J. Ruff, Antennas and feeds: mechanical design. Tech. rep., NRAO (2002). URL http://www.aoc.nrao.edu/evla/admin/reviews/feeds/feeds_files/Feedcone_Jim.pdf
 22. J. Ruff, Fiberglass laminating, evla c, s and l band feed horns. Tech. Rep. 23665S001, NRAO (2002)
 23. H.F. Barreiros, J.R. Soria, Análise estática: Projeto conjunto corneta do telescópio BINGO. Tech. rep., Analysis Engenharia & Consultoria (2018)
 24. M. Chen, G. Tsandoulas, IEEE Transactions on Antennas and Propagation **21**, 389 (1973). URL <https://ieeexplore.ieee.org/abstract/document/1140486>